

# Topological delocalization transitions and mobility edges in the nonreciprocal Maryland model

Longwen Zhou<sup>1,\*</sup> and Yongjian Gu<sup>1,†</sup>

<sup>1</sup>*College of Physics and Optoelectronic Engineering,  
Ocean University of China, Qingdao, China 266100*

(Dated: 2022-01-13)

Non-Hermitian effects could trigger spectrum, localization and topological phase transitions in quasiperiodic lattices. We propose a non-Hermitian extension of the Maryland model, which forms a paradigm in the study of localization and quantum chaos by introducing asymmetry to its hopping amplitudes. The resulting nonreciprocal Maryland model is found to possess a real-to-complex spectrum transition at a finite amount of hopping asymmetry, through which it changes from a localized phase to a mobility edge phase. Explicit expressions of the complex energy dispersions, phase boundaries and mobility edges are found. A topological winding number is further introduced to characterize the transition between different phases. Our work introduces a unique type of non-Hermitian quasicrystal, which admits exactly obtainable phase diagrams, mobility edges, and holding no extended phases at finite nonreciprocity in the thermodynamic limit.

## I. INTRODUCTION

Non-Hermitian topological matter has attracted great attention in the past decade (see [1–6] for reviews). Theoretically, these unique phases have been classified according to their symmetries and exceptional topologies [7–12]. Experimentally, non-Hermitian topological phases have been engineered in a broad range of physical platforms [13–26], yielding potential applications such as topological lasers [27–29] and high-performance sensors [30–33].

The localization problem in non-Hermitian systems was introduced early on by Hatano and Nelson [34], and followed up by a series of related studies [35–38]. In the Hatano-Nelson model, the asymmetry in the hopping amplitude of the one-dimensional Anderson model was found to be able to induce a transition from an insulator to a metallic phase. Recently, the development of non-Hermitian topological matter has re-evoked the interest in non-Hermitian systems with spatial aperiodicity. Specially, the interplay between non-Hermitian effects and quasiperiodic modulations has been found to induce rich patterns of localization-delocalization transitions, topological phase transitions and mobility edges in one-dimensional (1D) non-Hermitian quasicrystals (NHQCs) [39–63]. Typical systems considered in the study of 1D NHQCs include various extensions of the Aubry-André-Harper [41–44, 50], Fibonacci [57], Su-Schrieffer-Heeger [59], Kitaev chain [62] and Maryland [63] models. Localization and topological transitions induced by time-periodic driving fields have also been investigated in the context of Floquet NHQCs [64]. Another way to make a disordered system non-Hermitian is to couple it to the outside world by a lead, as explored earlier in [65].

In this work, we introduce a non-Hermitian extension of the quasiperiodic Maryland model [66–71] by adding nonreciprocity to its hopping amplitudes. The resulting system exhibits two distinct NHQC phases and a phase transition induced by the hopping asymmetry. We introduce our model in Sec. II and reveal its key features in Sec. III. Besides characterizing the real-to-complex spectrum transition and the delocalization transition from an insulator to a mobility edge phase with coexisting extended and localized states in Secs. III A and III B, we also introduce a topological winding number to describe different phases and transitions in the nonreciprocal Maryland model in Sec. III C. We summarize our results and discuss potential future work in Sec. IV.

## II. MODEL

The Maryland model describes particles hopping in a tight-binding lattice and subject to an unbounded onsite superlattice potential. Its Hamiltonian in position representation takes the form  $H_0 = \sum_n (J|n\rangle\langle n+1| + \text{H.c.} + V \tan(\pi\alpha n)|n\rangle\langle n|)$ . Here  $J$  is the nearest-neighbor (NN) hopping amplitude,  $V$  is the amplitude of onsite potential,  $n \in \mathbb{Z}$  is the lattice site index and  $\{|n\rangle\}$  forms a complete basis of the lattice.  $\alpha$  is chosen as an irrational number to realize quasiperiodic modulations. The Hermitian Maryland model  $H_0$  is first introduced as an integrable model to study localization problems in quantum chaotic systems [66–71]. Later, it is also utilized to understand the localization in higher dimensions [72–74] and topological features of integer quantum Hall effects [75]. Experimentally, the Maryland model might be realized in photonic systems by engineering the light propagation in polygonal optical waveguide lattices [76].

In this work, we focus on the localization problem in a non-Hermitian extension of the Maryland model, which is obtained by incorporating asymmetry into the hopping amplitudes of  $H_0$ . The Hamiltonian of the resulting sys-

\* zhoulw13@u.nus.edu

† guyj@ouc.edu.cn

tem, which is dubbed the nonreciprocal Maryland model (NRMM), takes the following form

$$H = J \sum_n (e^{-\gamma} |n\rangle \langle n+1| + e^{\gamma} |n+1\rangle \langle n|) + V \sum_n \tan(\pi\alpha n) |n\rangle \langle n|. \quad (1)$$

Here  $J, V, \gamma \in \mathbb{R}$ .  $\gamma$  measures the degree of asymmetry between left-to-right and right-to-left NN hopping amplitudes. We take the periodic boundary condition (PBC) for all calculations below by identifying  $|n\rangle = |n+L\rangle$ , where  $n = 1, 2, \dots, L$  and  $L$  is the length of lattice. When  $\alpha = p/q$  ( $p, q$  being coprime integers) is chosen to be a rational number and  $L$  is an integer multiple of  $q$ , the system is in the commensurate regime and under the PBC it is expected to hold charge density wave like states. In this work, we instead take  $\alpha = \frac{\sqrt{5}-1}{2}$ , i.e., the inverse golden ratio to yield a quasiperiodic potential. Inserting the expansion of state  $|\psi\rangle = \sum_n \psi_n |n\rangle$  into the eigenvalue equation  $H|\psi\rangle = E|\psi\rangle$ , we obtain

$$J(e^{-\gamma} \psi_{n+1} + e^{\gamma} \psi_{n-1}) + V \tan(\pi\alpha n) \psi_n = E \psi_n. \quad (2)$$

Here  $E$  is the energy of state  $|\psi\rangle$ , which is in general complex as  $H \neq H^\dagger$ .  $\psi_n \equiv \langle n|\psi\rangle$  represents the amplitude of right eigenvector  $|\psi\rangle$  on the  $n$ th lattice site. The solution of Eq. (2) under the PBC then yields all the possible eigenenergies and eigenstates of the NRMM. Note that in numerical calculations, we take a rational approximation for  $\alpha$  by setting  $\alpha \simeq F_l/F_{l+1}$ , where  $F_l$  and  $F_{l+1}$  are two adjacent elements of the Fibonacci sequence.

In the Hermitian limit ( $\gamma = 0$ ), due to the unbounded nature of onsite potential  $V_n = V \tan(\pi\alpha n)$ , all eigenstates of  $H$  are localized with energy-dependent localization lengths for irrational  $\alpha$  and  $V \neq 0$ . Away from the Hermitian limit, however, we find a nonreciprocity induced transition of the system from a localized phase with real spectrum to a mobility edge phase with complex spectrum at a finite  $\gamma = \gamma_c$ , which is thus of non-Hermitian origin. Note that the mobility edge phase means a phase in which extended and localized states coexist and are separated in their energies by a mobility edge. We present systematic characterizations of this transition and the resulting energy-dependent mobility edges in the following section.

### III. RESULTS

In this section, we investigate the spectrum, delocalization and topological transitions of the NRMM. In Sec. III A, we study the energies of NRMM and find a real-to-complex spectral transition at a finite hopping asymmetry  $\gamma = \gamma_c$ , whose expression as a function of the hopping amplitude and onsite potential is obtained. In Sec. III B, the spectrum transition is connected to a transition of the system from localized to mobility edge

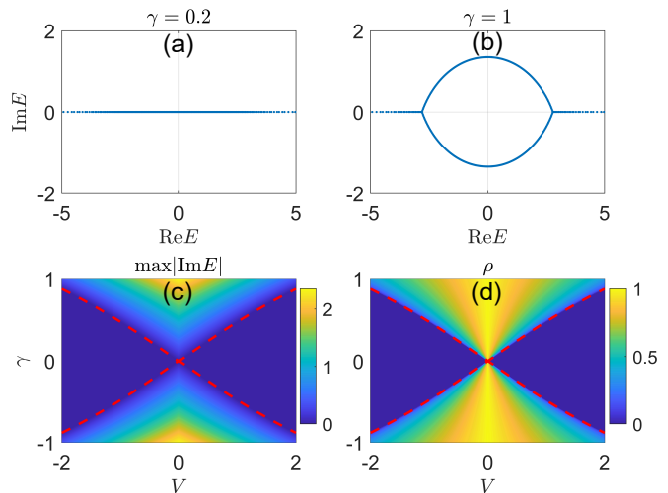


FIG. 1. Spectrum and DOS of NRMM under the PBC. System parameters are  $J = 1$ ,  $\alpha = \frac{\sqrt{5}-1}{2}$  for all panels, and the length of lattice is  $L = 377$ . (a) and (b) show two typical examples of the spectrum on the complex plane with  $V = 1$ . (c) and (d) show the maximal imaginary parts of eigenenergies  $\max|\text{Im}E|$  and DOS with complex energies  $\rho$  at different sets of  $(V, \gamma)$ . The red dashed lines in (c) and (d) highlight the boundaries between phases with real and complex spectrum, which are determined by Eq. (4).

phases. The mobility edge separating localized and extended states is further picked up and its expression is found to be energy-dependent. In Sec. III C, a topological winding number is introduced to distinguish phases with different transport nature and characterize the transitions between them in the NRMM, thus yielding a complete phase diagram. For ease of reference, we summarize our main results about the NRMM in Table I.

#### A. Real-to-complex spectrum transition

We first study the spectrum of NRMM by solving the eigenvalue Eq. (2). Two typical examples of the spectrum are presented in Figs. 1(a) and 1(b), where  $\text{Re}E$  and  $\text{Im}E$  refer to the real and imaginary parts of energy  $E$ , respectively. We observe that with weak hopping asymmetry  $\gamma$ , the eigenvalues of  $H$  could retain real. When  $\gamma$  goes beyond a critical value  $\gamma_c$ , a finite amounts of eigenenergies deviate from the real axis, and the spectrum undergoes a real-to-complex transition. After the transition, the complex part of eigenenergies develop a loop on the  $\text{Re}E$ - $\text{Im}E$  plane surrounding a base energy  $E_0 = 0$ . The points along the loop in Fig. 1(b) satisfy the equation

$$E_{\pm} = 2J \cos(\beta - i\gamma) \pm iV, \quad \beta \in [-\pi, \pi) \quad (3)$$

under the constraint  $\text{Im}E_- > \text{Im}E_+$ .

To find the critical point  $\gamma_c$  as a function of system parameters, we evaluate the maximum of imaginary parts of energy  $\max|\text{Im}E|$  and the density of states (DOS)

Phase	Localized	Mobility edge
<b>Condition</b>	$ 2J \sinh \gamma  <  V $	$ 2J \sinh \gamma  >  V $
<b>Spectrum</b>	Real	Complex (see Eq. (3))
<b>IPR</b>	$> 0$ for all states	$> 0$ and $\simeq 0$ coexist
<b>Mobility edge equation</b>	$\frac{V^2}{(2J \sinh \gamma)^2} + \frac{(\text{Re}E)^2}{(2J \cosh \gamma)^2} = 1$	
<b>Winding number</b>	$w = \int_0^{2\pi} \frac{d\theta}{2\pi i} \partial_\theta \ln \det[H(\theta) - E_0] = \begin{cases} 0 & \text{Localized} \\ \pm 1 & \text{Mobility edge} \end{cases}$	

TABLE I. Summary of results for the NRMM.  $J$ ,  $\gamma$  and  $V$  control the hopping amplitude, hopping asymmetry and onsite potential.  $E$  is the eigenenergy.  $H(\theta)$  is obtained from  $H$  in Eq. (1) by setting  $e^{\pm\gamma} \rightarrow e^{\pm\gamma \pm i\theta/L}$ , with  $L$  being the length of lattice. The base energy is set as  $E_0 = 0$  in the calculation of  $w$ .

with complex eigenvalues  $\rho$  at different  $V$  and  $\gamma$ , with results presented in Figs. 1(c) and 1(d). In numerical calculations, we count  $E$  as a complex eigenvalue if  $|\text{Im}E| > 10^{-5}$ . It is clear that once  $V \neq 0$ , we could obtain spectrum transitions from real to complex in the NRMM with the increase of  $|\gamma|$ . By setting  $\text{Im}E_{\pm} = 0$  in Eq. (3), we find the critical values of hopping asymmetry  $\gamma = \gamma_c$  where spectrum transitions happen, i.e.,

$$\gamma_c = \pm \text{arcsinh} \left( \frac{V}{2J} \right). \quad (4)$$

When  $|\gamma| < |\gamma_c|$ , all eigenvalues of  $H$  are found to be real, whereas a finite portion of the spectrum becomes complex for  $|\gamma| > |\gamma_c|$ . We plot these exact phase boundaries by red dashed lines in Figs. 1(c) and 1(d), and find that they are coincide with numerical calculations of the spectrum. Meanwhile, Eq. (4) provides us with a guideline for the study of transport nature of the NRMM, as will be discussed in the next subsection.

### B. Delocalization transition and mobility edge

In NHQCs, spectrum transitions usually accompany state transitions regarding their spatial profiles [41, 42]. In the NRMM, we also discover a transition from an insulator phase with no extended eigenstates to a mobility edge phase, in which extended and localized eigenstates coexist. To see this, we first inspect the inverse participation ratio (IPR), which is defined for the  $i$ th normalized eigenstate  $|\psi^i\rangle$  of  $H$  in the lattice representation as  $\text{IPR}_i = \sum_{n=1}^L |\psi_n^i|^4$ . Here the amplitude  $\psi_n^i = \langle n | \psi^i \rangle$  and  $i = 1, 2, \dots, L$ . In the localized phase, all eigenstates have finite IPRs. Extended states start to appear when the minimum of IPRs, denoted as  $\text{min(IPR)}$ , starts to approach zero.

In Fig. 2(a), we show the minimum, maximum and average of IPRs for the NRMM. It is clear that the  $\text{max(IPR)} \simeq 1$  due to the unbounded nature of the onsite potential  $V_n$ , which indicates that there are localized states at any hopping asymmetry in the limit  $L \rightarrow \infty$ . Notably, the  $\text{min(IPR)}$  decreases to zero when  $\gamma$  goes beyond a critical value  $\gamma_c$ , which happens to be coincide

with the critical point of spectrum transition in Eq. (4). Therefore, when the hopping asymmetry is tuned from below to above the critical point  $\gamma_c$ , the NRMM transforms from a localized phase with real spectrum to a mobility edge phase with complex spectrum. The number of extended states in the mobility edge phase further increases with the increase of  $\gamma$ , as hinted by the  $\text{ave(IPR)}$  in Fig. 2(a). In Fig. 2(b), we present the  $\text{min(IPR)}$  as a function of system parameters ( $V, \gamma$ ), and indeed observe two distinct phases characterized by  $\text{min(IPR)} > 0$  and  $\text{min(IPR)} \simeq 0$ . Their boundaries are highlighted by the red dashed lines and given exactly by Eq. (4). To the best of our knowledge, the NRMM contributes the first example of a 1D NHQC with only localized and mobility edge phases, but no metallic phases at any amounts of non-Hermiticity.

To give a more detailed look at the mobility edge, we show the IPRs of all eigenstates of the NRMM versus the real parts of their energies and the potential amplitude  $V$  (hopping asymmetry  $\gamma$ ) for two typical examples in Figs. 2(c) and 2(d). We observe that the states with  $\text{IPR} \simeq 0$  and  $\text{IPR} > 0$  are clearly separated in both figures. Moreover, with thorough numerical analysis, we find an equation that describes the mobility edge of the NRMM, i.e.,

$$\frac{V^2}{(2J \sinh \gamma)^2} + \frac{(\text{Re}E)^2}{(2J \cosh \gamma)^2} = 1. \quad (5)$$

Trajectories determined by this equation, presented by the magenta dashed lines in Figs. 2(c) and 2(d), separate states with vanishing and finite IPRs in the energy-parameter plane of the system. Moreover, the Eq. (5) is well-defined at finite  $V$  only if  $\gamma \neq 0$ . Therefore, mobility edges in the NRMM are solely originated from non-Hermitian effects encoded in the hopping asymmetry of the lattice.

### C. Topological invariant and phase diagram

In recent studies, a spectral winding number has been introduced to depict the transitions between different NHQC phases [41], following a strategy that is differ-

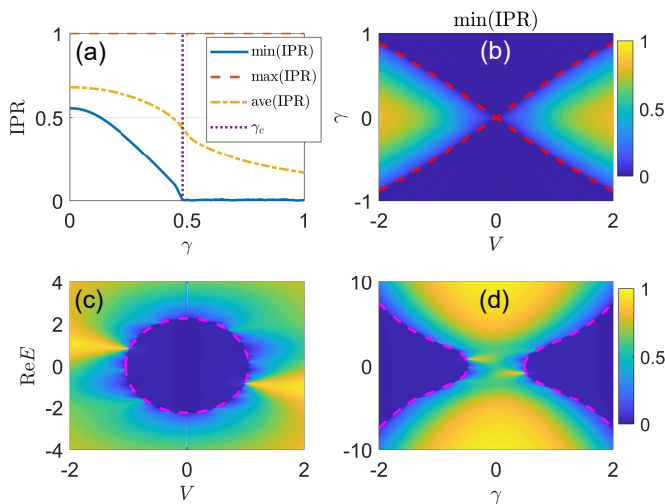


FIG. 2. IPRs of NRMM under the PBC. The length of lattice is  $L = 987$ . System parameters are  $J = 1$ ,  $\alpha = \frac{\sqrt{5}-1}{2}$  for all panels. In (a), the solid, dashed and dash-dotted lines show the minimum, maximum and average of IPRs versus the hopping asymmetry  $\gamma$  at  $V = 1$ . The crossing point of the dotted line and the horizontal axis corresponds to the critical value of  $\gamma = \gamma_c = \text{asinh}(V/2J) \approx 0.4812$ , where the system undergoes a transition from the localized to the mobility edge phase. (b) shows the minimum of IPRs at different parameters  $(V, \gamma)$ . The red dashed lines refer to the boundaries between localized and mobility edge phases, which are given by Eq. (4). The IPRs of all states versus the real parts of their energies and  $V$  ( $\gamma$ ) are shown in (c) ((d)) with  $\gamma = 0.5$  ( $V = 1$ ). The magenta dashed lines obtained following Eq. (5) are mobility edges separating extended and localized states.

ent from the topological characterization of Hermitian quasicrystals (see [77] for a review). The general idea is to incorporate a periodic parameter  $\theta$  into the Hamiltonian  $H$  of the system, usually achieved by imposing the twist boundary condition (flux insertion), and then track the spectral flow of the parameter-dependent Hamiltonian  $H(\theta)$  with respect to a certain base energy on the complex plane during the change of  $\theta$  over a cycle. If the spectrum of  $H(\theta)$  is real, all eigenvalues collapse onto the real axis and their winding number  $w$  must vanish with respect to any base energies. If  $H(\theta)$  possesses complex energies, their flow with respect to  $\theta$  could form loops around certain points on the complex plane, and the spectral winding number of  $H(\theta)$  around these points could be nonzero and quantized. The value of  $w$  jumps whenever the spectral of the system changes from real to complex, or vice versa. Therefore,  $w$  can be naturally employed as a topological order parameter to distinguish NHQC phases with real and complex eigenspectrum. Interestingly, it was found in some typical NHQC models [41, 64] that the real-complex spectral transition could go together with a localization-delocalization transition (with a possible exception reported in Ref. [61]). Therefore, we may adopt the same winding number to signify the emergence of mobility edge phase in our sys-

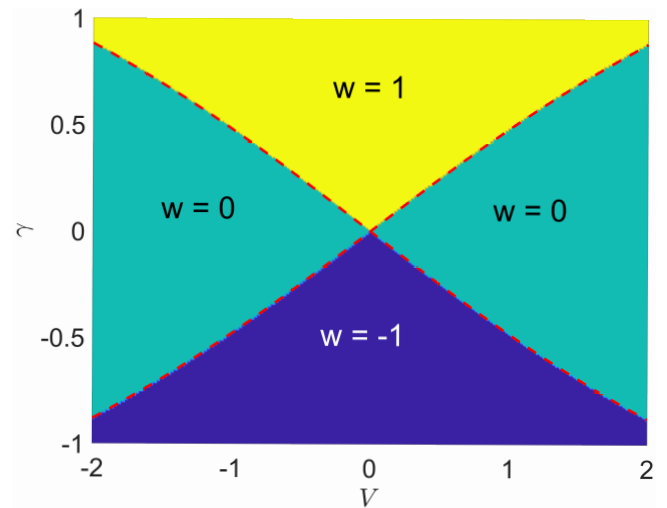


FIG. 3. Winding numbers of the NRMM. System parameters are  $J = 1$  and  $\alpha = \frac{\sqrt{5}-1}{2}$ . The length of lattice is  $L = 377$  with the twist boundary condition. Each region with a uniform color corresponds to a phase with common spectrum and transport features, whose winding number  $w$  is denoted explicitly therein. The red dashed lines separating different regions denote the phase boundaries obtained from Eq. (4).

tem, since the extended states therein are those whose energies possess nonvanishing imaginary parts.

For the NRMM, we construct a spectral winding number as

$$w = \frac{1}{2\pi i} \int_0^{2\pi} \partial_\theta \ln \det[H(\theta) - E_0] d\theta. \quad (6)$$

Here  $H(\theta)$  is obtained from  $H$  by letting  $e^{\pm\gamma} \rightarrow e^{\pm\gamma \pm i\theta/L}$  in Eq. (1), with  $L$  being the length of lattice. This winding number counts the number of times the spectrum of  $H(\theta)$  winds around the base energy  $E_0$  when  $\theta$  changes over a cycle from zero to  $2\pi$ . Referring to the spectrum presented in Fig. 1, we choose  $E_0 = 0$  in our calculation of  $w$  without loss of generality. It is clear that in the Hermitian region ( $\gamma = 0$ ) we have  $w = 0$ , since in this case  $H(\theta)$  has only real energies. At a finite hopping asymmetry  $\gamma = \gamma_c$ , we expect a quantized jump of  $w$  from zero to  $\pm 1$ , which should be accompanied by the spectrum transition of the NRMM from real to complex.

In Fig. 3, we present the winding number  $w$  of NRMM versus the onsite potential  $V$  and hopping nonreciprocity  $\gamma$ , which is obtained directly from Eq. (6). The red dashed lines in Fig. 3 highlight the exact phase boundaries, which are given by Eq. (4). We observe that the winding number  $w$  takes a quantized change when crossing the border between two NHQC phases, and remain constant elsewhere. More specially, we find  $w = 0$  when the system is prepared in the localized phase with real spectrum, and  $w = \pm 1$  if the system moves into the mobility edge phase with complex spectrum. These observations confirm that the topological winding number  $w$  can

indeed be utilized to discriminate the NHQC phases of NRMM with distinct spectrum and transport nature, and characterize the transitions between them in the meantime.

For completeness, we have checked other values of the irrational parameter  $\alpha$  (e.g.,  $\alpha = (\sqrt{5} + 1)/2, 1/\sqrt{2}$ ) in our calculations of spectrum, IPRs and winding numbers of the NRMM. The results we obtained are all consistent with those reported in Figs. 1–3, which implies that the conclusion we drew from this section is general to other incommensurate values of the onsite potential in Eq. (1).

#### IV. SUMMARY AND DISCUSSION

In this work, we uncover non-Hermiticity induced spectral, localization and topological phase transitions in the nonreciprocal Maryland model. A transformation of the system from a localized phase with real spectrum to a mobility edge phase with complex spectrum can be obtained only if there are finite amounts of hopping asymmetry. The equations satisfied by the complex spectrum, phase boundaries and energy-dependent mobility edges are found exactly. A topological order parameter is further employed to build the phase diagram and characterize transitions between different NHQC phases. Notably, due to the unbounded nature of onsite potential in the NRMM, we find no extended phases at any finite hopping nonreciprocity, which is distinct from the situation found in a Maryland model with complex onsite potential [63]. Our study thus enriches the family of NHQCs by unveiling a particular type of system with only localized and mobility edge phases, whose properties can be characterized exactly.

In future work, it would be interesting to consider many-body effects in Maryland-type NHQCs and investigate their dynamical properties. The interplay between non-Hermiticity and quantum chaos in the NRMM can further be studied following the mapping discussed in Appendix A. In this work, our calculations are performed under the PBC and the non-Hermitian skin effects (NHSEs) [78–82] are expected to have no impacts on the results. Under the open boundary condition, the non-reciprocal hoppings in our model could possibly induce non-Hermitian skin modes. Recently, it was shown that (de)localization transitions and (pseudo) mobility edges could even emerge in clean systems due to the NHSEs, and topological characterizations of these intriguing phenomena have been proposed [83]. Therefore, it is expected that in the presence of both NHSEs and spatial quasiperiodicity, richer patterns of spectrum, localization and topological transitions could appear in generic NHQCs, which deserve more thorough explorations.

#### ACKNOWLEDGMENTS

L.Z. is supported by the National Natural Science Foundation of China (Grant No. 11905211), the China Postdoctoral Science Foundation (Grant No. 2019M662444), the Fundamental Research Funds for the Central Universities (Grant No. 841912009), the Young Talents Project at Ocean University of China (Grant No. 861801013196), and the Applied Research Project of Postdoctoral Fellows in Qingdao (Grant No. 861905040009).

#### Appendix A: NRMM and Floquet system

The Hermitian Maryland model can be mapped to a mathematically equivalent Floquet system [66]. A similar mapping can also be constructed for the NRMM, which may serve as an entrance for the study of the interplay between non-Hermiticity and quantum chaos.

We start by rewriting the eigenvalue Eq. (2) as

$$\frac{E}{V}\psi_n - \frac{e^{-\gamma}}{V}\psi_{n+1} - \frac{e^{\gamma}}{V}\psi_{n-1} = \tan(\pi\alpha n)\psi_n, \quad (\text{A.1})$$

where we have set  $J = 1$  as the unit of energy. Multiplying the imaginary unit  $i$  from both sides of Eq. (A.1), we obtain

$$\frac{V\psi_n - i(E\psi_n - e^{-\gamma}\psi_{n+1} - e^{\gamma}\psi_{n-1})}{V\psi_n + i(E\psi_n - e^{-\gamma}\psi_{n+1} - e^{\gamma}\psi_{n-1})} = e^{-i2\pi\alpha n}. \quad (\text{A.2})$$

For a 1D quasicrystal, the amplitude  $\psi_n$  can be expressed as a superposition of plane waves [63], i.e.,

$$\psi_n = \sum_{\ell} \varphi_{\ell} e^{ik_{\ell}n}. \quad (\text{A.3})$$

Here for any  $\ell \neq \ell'$ , the difference between wave numbers  $k_{\ell}$  and  $k_{\ell'}$  is an integer multiple of  $2\pi\alpha$ . Taking  $\psi_n$  as amplitudes, we can further construct a series

$$\begin{aligned} \Psi(x) &= \sum_n \psi_n e^{inx} = \sum_{\ell} \varphi_{\ell} \sum_n e^{i(x+k_{\ell})n} \\ &= 2\pi \sum_{\ell, n} \varphi_{\ell} \delta(x + k_{\ell} - 2\pi n), \end{aligned} \quad (\text{A.4})$$

where we used the Poisson summation formula to arrive at the last equality. If we now multiply  $e^{inx}$  to Eq. (A.2) and take the summation over  $n$ , we will obtain with the help of Eq. (A.4) that

$$\begin{aligned} &\left[1 - i\frac{E}{V} + i\frac{2}{V}\cos(x - i\gamma)\right] \Psi(x) \\ &= \left[1 + i\frac{E}{V} - i\frac{2}{V}\cos(x - 2\pi\alpha - i\gamma)\right] \Psi(x - 2\pi\alpha). \end{aligned} \quad (\text{A.5})$$

To make the connection between the NRMM and its

Floquet equivalent more transparent, we introduce the function

$$\Phi(x) = \left[ 1 + i\frac{E}{V} - i\frac{2}{V} \cos(x - i\gamma) \right] \Psi(x). \quad (\text{A.6})$$

Using Eq. (A.6), we can express Eq. (A.5) as

$$\Phi(x) = \frac{1 + i\frac{E}{V} - i\frac{2}{V} \cos(x - i\gamma)}{1 - i\frac{E}{V} + i\frac{2}{V} \cos(x - i\gamma)} \Phi(x - 2\pi\alpha). \quad (\text{A.7})$$

Performing the Taylor expansion of  $\Phi(x - 2\pi\alpha)$ , we find

$$\Phi(x - 2\pi\alpha) = \sum_n \frac{(-2\pi\alpha)^n}{n!} \frac{\partial^n \Phi(x)}{\partial x^n} = e^{-2\pi\alpha\partial_x} \Phi(x). \quad (\text{A.8})$$

Meanwhile, we can introduce a function  $\mathcal{K}(x)$  that satisfies

$$\begin{aligned} e^{-i\mathcal{K}(x)} &= \cos[\mathcal{K}(x)] - i \sin[\mathcal{K}(x)] \\ &= \frac{1 + i\frac{E}{V} - i\frac{2}{V} \cos(x - i\gamma)}{1 - i\frac{E}{V} + i\frac{2}{V} \cos(x - i\gamma)}, \end{aligned} \quad (\text{A.9})$$

yielding

$$\mathcal{K}(x) = 2 \arctan \left[ \frac{2}{V} \cos(x - i\gamma) - \frac{E}{V} \right]. \quad (\text{A.10})$$

Plugging Eqs. (A.8)–(A.10) into Eq. (A.7), we finally obtain

$$\Phi(x) = e^{-i\mathcal{K}(x)} e^{-2\pi\alpha\partial_x} \Phi(x), \quad (\text{A.11})$$

which can be interpreted as describing the one-period evolution of a particle with linear dispersion in its kinetic energy  $-2\pi\alpha i\partial_x$  and subject to a delta-kicking potential  $\mathcal{K}(x)$  within the driving period  $T = 1$ . The corresponding Schrödinger equation takes the form

$$i\partial_t \Phi = -2\pi\alpha i\partial_x \Phi + \mathcal{K}(x) \sum_{m \in \mathbb{Z}} \delta(t - m) \Phi, \quad (\text{A.12})$$

and the quasienergy can be viewed as  $\varepsilon = 0$ . The above analysis establishes a relationship between the spectrum nature of NRMM and the dynamics of a periodically kicked particle with linearized kinetic energy.

- 
- [1] R. El-Ganainy, K. G. Makris, M. Khajavikhan, Z. H. Musslimani, S. Rotter, and D. N. Christodoulides, Non-Hermitian physics and PT symmetry, *Nat. Phys.* **14**, 11-19 (2018).
- [2] V. M. Martinez Alvarez, J. E. Barrios Vargas, M. Berdakin, and L. E. F. Foa Torres, Topological states of non-Hermitian systems, *Eur. Phys. J. Spec. Top.* **227**, 1295 (2018).
- [3] A. Ghatak and T. Das, New topological invariants in non-Hermitian systems, *J. Phys.: Condens. Matter* **31**, 263001 (2019).
- [4] C. Coulais, R. Fleury, and J. van Wezel, Topology and broken Hermiticity, *Nat. Phys.* **17**, 9-13 (2021).
- [5] E. J. Bergholtz, J. C. Budich, and F. K. Kunst, Exceptional topology of non-Hermitian systems, *Rev. Mod. Phys.* **93**, 015005 (2021).
- [6] Y. Ashida, Z. Gong, and M. Ueda, Non-Hermitian physics, *Adv. Phys.* **69**, 249-435 (2021).
- [7] H. Shen, B. Zhen, and L. Fu, Topological band theory for non-Hermitian Hamiltonians, *Phys. Rev. Lett.* **120**, 146402 (2018).
- [8] Z. Gong, Y. Ashida, K. Kawabata, K. Takasan, S. Higashikawa, and M. Ueda, Topological phases of non-Hermitian systems, *Phys. Rev. X* **8**, 031079 (2018).
- [9] K. Kawabata, K. Shiozaki, M. Ueda and M. Sato, Symmetry and topology in non-Hermitian physics, *Phys. Rev. X* **9**, 041015 (2019).
- [10] H. Zhou and J. Y. Lee, Periodic table for topological bands with non-Hermitian symmetries, *Phys. Rev. B* **99**, 235112 (2019).
- [11] C. C. Wojcik, X. Sun, T. Bzdušek, and S. Fan, Homotopy characterization of non-Hermitian Hamiltonians, *Phys. Rev. B* **101**, 205417 (2020).
- [12] K. Shiozaki and S. Ono, Symmetry indicator in non-Hermitian systems, *Phys. Rev. B* **104**, 035424 (2021).
- [13] Y. Xu, S.-T. Wang, and L.-M. Duan, Weyl Exceptional Rings in a Three-Dimensional Dissipative Cold Atomic Gas, *Phys. Rev. Lett.* **118**, 045701 (2017).
- [14] J. Li, A. K. Harter, J. Liu, L. d. Melo, Y. N. Joglekar, and L. Luo, Observation of parity-time symmetry breaking transitions in a dissipative Floquet system of ultracold atoms, *Nat. Commun.* **10**, 855 (2019).
- [15] W. Gou, T. Chen, D. Xie, T. Xiao, T.-S. Deng, B. Gadway, W. Yi, and B. Yan, Tunable Nonreciprocal Quantum Transport through a Dissipative Aharonov-Bohm Ring in Ultracold Atoms, *Phys. Rev. Lett.* **124**, 070402 (2020).
- [16] J. M. Zeuner, M. C. Rechtsman, Y. Plotnik, Y. Lumer, S. Nolte, M. S. Rudner, M. Segev, and A. Szameit, Observation of a Topological Transition in the Bulk of a Non-Hermitian System, *Phys. Rev. Lett.* **115**, 040402 (2015).
- [17] S. Weimann, M. Kremer, Y. Plotnik, Y. Lumer, S. Nolte, K. G. Makris, M. Segev, M. C. Rechtsman, and A. Szameit, Topologically protected bound states in photonic parity-time-symmetric crystals, *Nat. Mater.* **16**, 433-438 (2017).
- [18] K. Wang, X. Qiu, L. Xiao, X. Zhan, Z. Bian, B. C. Sanders, W. Yi, and P. Xue, Observation of emergent momentum-time skyrmions in parity-time-symmetric non-unitary quench dynamics, *Nat. Commun.* **10**, 2293 (2019).
- [19] L. Xiao, T. Deng, K. Wang, G. Zhu, Z. Wang, W. Yi, and P. Xue, Non-Hermitian bulk-boundary correspondence in quantum dynamics, *Nat. Phys.* **16**, 761-766 (2020).
- [20] T. Hofmann, T. Helbig, F. Schindler, N. Salgo, M. Brzezina, M. Greiter, T. Kiessling, D. Wolf, A. Vollhardt, A. Kabaš, C. H. Lee, A. Bilušić, R. Thomale, and T. Neupert, Reciprocal skin effect and its realization in a

- topoelectrical circuit, *Phys. Rev. Res.* **2**, 023265 (2020).
- [21] T. Helbig, T. Hofmann, S. Imhof, M. Abdelghany, T. Kiessling, L. W. Molenkamp, C. H. Lee, A. Szameit, M. Greiter, and R. Thomale, Generalized bulk-boundary correspondence in non-Hermitian topoelectrical circuits, *Nat. Phys.* **16**, 747-750 (2020).
- [22] S. Liu, S. Ma, C. Yang, L. Zhang, W. Gao, Y. J. Xiang, T. J. Cui, and S. Zhang, Gain- and Loss-Induced Topological Insulating Phase in a Non-Hermitian Electrical Circuit, *Phys. Rev. Appl.* **13**, 014047 (2020).
- [23] W. Zhu, X. Fang, D. Li, Y. Sun, Y. Li, Y. Jing, and H. Chen, Simultaneous Observation of a Topological Edge State and Exceptional Point in an Open and Non-Hermitian Acoustic System, *Phys. Rev. Lett.* **121**, 124501 (2018).
- [24] C. Shen, J. Li, X. Peng, and S. A. Cummer, Synthetic exceptional points and unidirectional zero reflection in non-Hermitian acoustic systems, *Phys. Rev. Mater.* **2**, 125203 (2018).
- [25] H. Gao, H. Xue, Q. Wang, Z. Gu, T. Liu, J. Zhu, and B. Zhang, Observation of topological edge states induced solely by non-Hermiticity in an acoustic crystal, *Phys. Rev. B* **101**, 180303(R) (2020).
- [26] Y. Wu, W. Liu, J. Geng, X. Song, X. Ye, C.-K. Duan, X. Rong, and J. Du, Observation of parity-time symmetry breaking in a single-spin system, *Science* **364**, 878-880 (2019).
- [27] G. Harari, M. A. Bandres, Y. Lumer, M. C. Rechtsman, Y. D. Chong, M. Khajavikhan, D. N. Christodoulides, and M. Segev, Topological insulator laser: Theory. *Science* **359**, 4003 (2018).
- [28] M. A. Bandres, S. Wittek, G. Harari, M. Parto, J. Ren, M. Segev, D. N. Christodoulides, and M. Khajavikhan, Topological insulator laser: Experiments. *Science* **359**, 4005 (2018).
- [29] Y. V. Kartashov and D. V. Skryabin, Two-Dimensional Topological Polariton Laser, *Phys. Rev. Lett.* **122**, 083902 (2019).
- [30] J. Wiersig, Enhancing the Sensitivity of Frequency and Energy Splitting Detection by Using Exceptional Points: Application to Microcavity Sensors for Single-Particle Detection, *Phys. Rev. Lett.* **112**, 203901 (2014).
- [31] H. Hodaei, A. U. Hassan, S. Wittek, H. Garcia-Gracia, R. El-Ganainy, D. N. Christodoulides, and M. Khajavikhan, Enhanced sensitivity at higher-order exceptional points, *Nature* **548**, 187-191 (2017).
- [32] W. Chen, S. K. Özdemir, G. Zhao, J. Wiersig, and L. Yang, Exceptional points enhance sensing in an optical microcavity, *Nature* **548**, 192-196 (2017).
- [33] H.-K. Lau and A. A. Clerk, Fundamental limits and non-reciprocal approaches in non-Hermitian quantum sensing, *Nat. Commun.* **9**, 4320 (2018).
- [34] N. Hatano and D. R. Nelson, Localization Transitions in Non-Hermitian Quantum Mechanics, *Phys. Rev. Lett.* **77**, 570 (1996).
- [35] N. Hatano and D. R. Nelson, Vortex pinning and non-Hermitian quantum mechanics, *Phys. Rev. B* **56**, 8651 (1997).
- [36] J. Feinberg and A. Zee, Non-Hermitian localization and delocalization, *Phys. Rev. E* **59**, 6433 (1999).
- [37] J. Feinberg and A. Zee, Spectral curves of non-hermitian hamiltonians, *Nucl. Phys. B* **552**, 599-623 (1999).
- [38] N. Hatano and J. Feinberg, Chebyshev-polynomial expansion of the localization length of Hermitian and non-Hermitian random chains, *Phys. Rev. E* **94**, 063305 (2016).
- [39] A. Jazaeri and I. I. Satija, Localization transition in incommensurate non-Hermitian systems, *Phys. Rev. E* **63**, 036222 (2001).
- [40] Q. Zeng, S. Chen, and R. Lü, Anderson localization in the non-Hermitian Aubry-André-Harper model with physical gain and loss, *Phys. Rev. A* **95**, 062118 (2017).
- [41] S. Longhi, Topological Phase Transition in non-Hermitian Quasicrystals, *Phys. Rev. Lett.* **122**, 237601 (2019).
- [42] H. Jiang, L. Lang, C. Yang, S. Zhu, and S. Chen, Interplay of non-Hermitian skin effects and Anderson localization in nonreciprocal quasiperiodic lattices, *Phys. Rev. B* **100**, 054301 (2019).
- [43] S. Longhi, Metal-insulator phase transition in a non-Hermitian Aubry-André-Harper model, *Phys. Rev. B* **100**, 125157 (2019).
- [44] T. Liu, H. Guo, Y. Pu, and S. Longhi, Generalized Aubry-André self-duality and mobility edges in non-Hermitian quasiperiodic lattices, *Phys. Rev. B* **102**, 024205 (2020).
- [45] Y. Liu, X.-P. Jiang, J. Cao, and S. Chen, Non-Hermitian mobility edges in one-dimensional quasicrystals with parity-time symmetry, *Phys. Rev. B* **101**, 174205 (2020).
- [46] Q. Zeng, Y. Yang, and R. Lü, Topological phases in one-dimensional nonreciprocal superlattices, *Phys. Rev. B* **101**, 125418 (2020).
- [47] Q. Zeng, Y. Yang, and Y. Xu, Topological phases in non-Hermitian Aubry-André-Harper models, *Phys. Rev. B* **101**, 020201(R) (2020).
- [48] Q. Zeng and Y. Xu, Winding numbers and generalized mobility edges in non-Hermitian systems, *Phys. Rev. Res.* **2**, 033052 (2020).
- [49] L. Zhai, S. Yin, and G. Huang, Many-body localization in a non-Hermitian quasiperiodic system, *Phys. Rev. B* **102**, 064206 (2020).
- [50] S. Longhi, Phase transitions in a non-Hermitian Aubry-André-Harper model, *Phys. Rev. B* **103**, 054203 (2021).
- [51] Y. Liu, Y. Wang, Z. Zheng, and S. Chen, Exact non-Hermitian mobility edges in one-dimensional quasicrystal lattice with exponentially decaying hopping and its dual lattice, *Phys. Rev. B* **103**, 134208 (2021).
- [52] Y. Liu, Y. Wang, X. Liu, Q. Zhou, and S. Chen, Exact mobility edges, PT-symmetry breaking, and skin effect in one-dimensional non-Hermitian quasicrystals, *Phys. Rev. B* **103**, 014203 (2021).
- [53] Z. Xu and S. Chen, Dynamical evolution in a one-dimensional incommensurate lattice with PT symmetry, *Phys. Rev. A* **103**, 043325 (2021).
- [54] X. Cai, Boundary-dependent self-dualities, winding numbers, and asymmetrical localization in non-Hermitian aperiodic one-dimensional models, *Phys. Rev. B* **103**, 014201 (2021).
- [55] L. Tang, G. Zhang, L. Zhang, and D. Zhang, Localization and topological transitions in non-Hermitian quasiperiodic lattices, *Phys. Rev. A* **103**, 033325 (2021).
- [56] T. Liu, S. Cheng, H. Guo, and X. Gao, Fate of Majorana zero modes, exact location of critical states, and unconventional real-complex transition in non-Hermitian quasiperiodic lattices, *Phys. Rev. B* **103**, 104203 (2021).
- [57] L. Zhai, G. Huang, and S. Yin, Cascade of the delocalization transition in a non-Hermitian interpolating Aubry-André-Fibonacci chain, *Phys. Rev. B* **104**, 014202 (2021).

- [58] X. Xia, K. Huang, S. Wang, and X. Li, A new class of exact mobility edges in non-Hermitian quasiperiodic models, arXiv:2105.12640.
- [59] L. Zhou and W. Han, Non-Hermitian quasicrystal in dimerized lattices, *Chin. Phys. B* **30**, 100308 (2021).
- [60] Y. Liu, Q. Zhou, and S. Chen, Localization transition, spectrum structure, and winding numbers for one-dimensional non-Hermitian quasicrystals, *Phys. Rev. B* **104**, 024201 (2021).
- [61] A. P. Acharya, A. Chakrabarty, and D. K. Sahu, Localization, PT-Symmetry Breaking and Topological Transitions in non-Hermitian Quasicrystals, arXiv:2108.03181.
- [62] X. Cai, Localization and topological phase transitions in non-Hermitian Aubry-André-Harper models with  $p$ -wave pairing, *Phys. Rev. B* **103**, 214202 (2021).
- [63] S. Longhi, Non-Hermitian Maryland model, *Phys. Rev. B* **103**, 224206 (2021).
- [64] L. Zhou, Floquet engineering of topological localization transitions and mobility edges in one-dimensional non-Hermitian quasicrystals, *Phys. Rev. Research* **3**, 033184 (2021).
- [65] H. Kunz and B. Shapiro, Statistics of resonances in a semi-infinite disordered chain, *Phys. Rev. B* **77**, 054203 (2008).
- [66] D. B. Grempel, S. Fishman, and B. E. Prange, Localization in an Incommensurate Potential: An Exactly Solvable Model, *Phys. Rev. Lett.* **49**, 833 (1982).
- [67] S. Fishman, D. R. Grempel, and R. E. Prange, Chaos, Quantum Recurrences, and Anderson Localization, *Phys. Rev. Lett.* **49**, 509 (1982).
- [68] D. R. Grempel, R. E. Prange, and S. Fishman, Quantum dynamics of a nonintegrable system, *Phys. Rev. A* **29**, 1639 (1984).
- [69] M. V. Berry, Incommensurability in an Exactly-Soluble Quantal and Classical Model for a Kicked Rotator, *Physica*, 10D, **369** (1984).
- [70] B. Simon, Almost periodic Schrödinger operators IV. The Maryland model, *Ann. Phys.* **159**, 157 (1985).
- [71] F. M. Izrailev, Simple models of quantum chaos: Spectrum and eigenfunctions, *Phys. Rep.* **196**, 299 (1990).
- [72] J. Bellissard, R. Lima and E. Scoppola, Localization in  $\nu$ -Dimensional Incommensurate Structures, *Comm. Math. Phys.* **88**, 465 (1983).
- [73] A. L. Figotin and L. A. Pastur, An Exactly Solvable model of a Multidimensional Incommensurate Structure, *Comm. Math. Phys.* **95**, 401 (1984).
- [74] S. Fishman, D. R. Grempel and R. E. Prange, Localization in a  $d$ -Dimensional Incommensurate Structure, *Phys. Rev. B* **29**, 4272 (1984).
- [75] S. Ganeshan, K. Kechedzhi, and S. Das Sarma, Critical integer quantum Hall topology and the integrable Maryland model as a topological quantum critical point, *Phys. Rev. B* **90**, 041405 (2014).
- [76] S. Longhi, Maryland model in optical waveguide lattices, *Opt. Lett.* **46**, 637-640 (2021).
- [77] O. Zilberberg, Topology in quasicrystals, *Opt. Mater. Express* **11**, 1143 (2021).
- [78] T. E. Lee, Anomalous Edge State in a Non-Hermitian Lattice, *Phys. Rev. Lett.* **116**, 133903 (2016).
- [79] S. Yao and Z. Wang, Edge States and Topological Invariants of Non-Hermitian Systems, *Phys. Rev. Lett.* **121**, 086803 (2018).
- [80] F. K. Kunst, E. Edvardsson, J. C. Budich, and E. J. Bergholtz, Biorthogonal Bulk-Boundary Correspondence in Non-Hermitian Systems, *Phys. Rev. Lett.* **121**, 026808 (2018).
- [81] V. M. Martinez Alvarez, J. E. Barrios Vargas, and L. E. F. Foa Torres, Non-Hermitian robust edge states in one dimension: anomalous localization and eigenspace condensation at exceptional points, *Phys. Rev. B* **97**, 121401(R) (2018).
- [82] C. H. Lee and R. Thomale, Anatomy of skin modes and topology in non-Hermitian systems, *Phys. Rev. B* **99**, 201103(R) (2019).
- [83] S. Mu, L. Zhou, L. Li, and J. Gong, Non-Hermitian pseudo mobility edge in a coupled chain system, arXiv:2111.11914.